# Increased Atmospheric $CO_2$: Zonal and Seasonal Estimates of the Effect on the Radiation Energy Balance and Surface Temperature

V. RAMANATHAN

*National Center for Atmospheric Research, Boulder, Colorado 80307*

M. S. LIAN AND R. D. CESS

*Laboratory for Planetary Atmospheres Research, State University of New York Stony Brook, New York 11794*

The climatic effects of increased atmospheric $CO_2$ are discussed in the context of the effect upon two basic components of the climate system, namely, (1) latitudinal and seasonal radiative heating of the surface-troposphere system and (2) the enhancement of latitudinal and seasonal surface temperatures. Radiative transfer model calculations show that the radiative heating of the surface-troposphere system (caused by increased $CO_2$) undergoes substantial latitudinal and seasonal variations. The seasonal variations are most pronounced at high latitudes. The increased $CO_2$ heating of the surface and troposphere is significantly different for clear sky and overcast sky conditions. These $CO_2$ heating calculations were then incorporated within a seasonal energy balance climate model for the northern hemisphere. Despite the significant seasonal variations in surface-troposphere heating due to increased $CO_2$, the seasonal model results, when annually averaged over all latitudes, yield essentially the same $CO_2$-induced increase in hemispherical mean surface temperature as does an annual energy balance model. The seasonal model, however, shows a strong seasonal variation at high latitudes for the increase in zonal surface temperature due to increased atmospheric $CO_2$. For example, the $CO_2$-induced enhancement in the zonal surface temperature for 80°–90°N is more than 3 times as great in the summer as in the winter.

## 1. INTRODUCTION

A number of published model studies have examined the climatic effects of increased atmospheric $CO_2$ concentrations. These studies have employed a hierarchy of climate models, including the one-dimensional radiative-convective model (*Manabe and Wetherald* [1967], *Schneider* [1975], and *Augustsson and Ramanathan* [1977], as well as several others), the two-dimensional zonal model [*Sellers*, 1974; *Lee and Snell*, 1977; *Ohring and Adler*, 1978], and the three-dimensional general circulation model [*Manabe and Wetherald*, 1975]. All of these model studies show that increased $CO_2$ would produce an increase in surface and tropospheric temperatures.

The computed warming is caused by the increase in $CO_2$ radiative heating of the surface-troposphere system, which in turn is due to the enhancement of the $CO_2$ longwave opacity. As was discussed by *Augustsson and Ramanathan* [1977], the enhancement of the $CO_2$ longwave opacity occurs in the 12- to 18-$\mu$m, 9- to 10-$\mu$m, and 7.6-$\mu$m spectral regions. The radiative heating of the surface is due to the increased downward emission by tropospheric $CO_2$, while the radiative heating of the troposphere is due to the following two processes: first, through the increased absorption of the emitted surface and cloud radiation and, second, through the increased downward emission from stratospheric $CO_2$. These radiative heating processes are strongly dependent upon the atmospheric temperature and humidity distributions (the dependence on the humidity is due to the overlapping of the $CO_2$ and $H_2O$ longwave bands). This temperature and humidity dependence of the $CO_2$ radiative effects, when considered in conjunction with the observed latitudinal and seasonal variations in atmospheric temperature and humidity, clearly suggests that the radiative effects of increased $CO_2$ should be a function of both latitude and season.

The importance of this aspect of the $CO_2$-climate problem cannot be inferred from published studies concerning enhanced $CO_2$, since these studies do not provide latitudinal and seasonal estimates of the $CO_2$ radiative heating rates. Estimates of this sort are of intrinsic scientific interest and, more importantly, are essential for interpreting the results of future three-dimensional model studies of the $CO_2$-climate problem in terms of isolating the effects produced by direct radiative effects from those produced by feedback mechanisms within the model.

Another aspect of the $CO_2$-climate problem concerns seasonal climatic effects. The major purpose of the present study is to estimate the latitudinal and seasonal radiative heating effects due to enhanced $CO_2$, as discussed above, and then to incorporate these results within a seasonal climate model, so as to estimate the seasonal climatic consequences of increased atmospheric $CO_2$. Toward this goal, we discuss here the climatic effects of increased $CO_2$ within the context of two basic components of the climate system, namely, (1) the latitudinal and seasonal radiative energy balance and radiative heating rates and (2) the latitudinal and seasonal surface temperatures. Our discussions are based upon results computed from models, and hence the conclusions we arrive at are subjected to the usual caveats that apply to model studies.

First, we will present results for the following components of the latitudinal and seasonal radiative effects of increased $CO_2$: (1) radiative energy budget of the earth-troposphere system, (2) radiative heating of the surface and troposphere, (3) stratospheric influence on the computed heating rates, and (4) differences between clear sky and overcast sky heating rates. These radiative effects of increased $CO_2$ are computed as a function of latitude and season by adopting the radiative transfer model described by *Ramanathan and Dickinson* [1979]. For these calculations, tropospheric temperatures are held fixed at the observed values, and we compute the radiative heating of the surface-troposphere system due to increased $CO_2$ after allowing for departure of stratospheric temperatures from the observed values.

Next, we employ the surface-troposphere radiative heating,



Paper number 9C0229.
0148-0227/79/009C-0229$01.00

computed as described above, within the seasonal energy balance climate model of *Lian* [1978] for the northern hemisphere in order to estimate the zonal and seasonal change in surface temperature due to increased $CO_2$. Upon averaging these surface temperature results both annually and latitudinally, we can additionally determine the effect of increased $CO_2$ upon the annual hemispherical mean surface temperature in order to compare seasonal and annual climate model predictions.

## 2. Description of the Models

In this section we first describe the model adopted for computing the effects of increased $CO_2$ on the radiative energy budget, and we then describe the seasonal climate model used for computing the effects on surface temperature.

### a. *Radiative Transfer Model*

The model used for this study is described in detail by *Ramanathan and Dickinson* [1979]. This model is based on that developed by *Ramanathan* [1976] but with major modifications, the details of which are described in the appendix.

The calculations use latitudinally and seasonally varying observed distributions of temperature, pressure, ozone mixing ratio, three effective cloud layers, and albedos for the surface and clouds. The longwave cooling (or heating), the solar heating within the stratosphere, and the net longwave and solar fluxes at the tropopause and at the surface are calculated. The usual convention of denoting the upward and downward fluxes, respectively, as positive and negative quantities is adopted, the net flux being given by the sum of the upward and downward fluxes. The sum of the net longwave and solar fluxes is referred to in the text as the net radiative flux. The solar and longwave fluxes and heating rates are calculated for each month of a season, and the three monthly values are then averaged to obtain the seasonal values. These calculated solar and longwave quantities are taken as the ambient or 'unperturbed' values. The $CO_2$ mixing ratio in the unperturbed atmosphere is assumed to be 320 ppm (by volume).

For the perturbed atmosphere, i.e., the atmosphere with increased $CO_2$, the change in stratospheric temperature from the unperturbed state is computed first (the adopted procedure for calculating stratospheric temperature change is described later). Then the difference in the net radiative flux, between the perturbed and unperturbed atmosphere, is computed both at the surface and at the tropopause. Roughly 95% of the change in the net radiative flux is due to the change in the net longwave flux, and hence we will not discuss individual changes in the longwave and solar fluxes.

The net radiative flux at the tropopause and at the surface decreases due to increased $CO_2$, and this decrease of course denotes a heating. The decrease of the flux at the tropopause denotes a heating of the entire surface-troposphere system; the flux decrease at the surface denotes a heating of the surface, while the difference between the above two quantities gives the heating of the troposphere alone.

The stratospheric temperature change due to increased $CO_2$ is calculated from radiative energy balance considerations. The latitudinal variation of the change cannot be determined precisely without an interactive dynamical model. However, we can consider three scenarios which put likely bounds on this change. The first scenario assumes no change in stratospheric temperature. In the second scenario we assume negligible dynamical feedback effects on temperature change. In this case, stratospheric temperatures are adjusted from the unperturbed values until the perturbations in $CO_2$ solar and longwave heating (or cooling) rates within the stratosphere vanish. In other words, we assume that the stratosphere undergoes primarily local radiative adjustments in response to heating perturbations. This case is referred to as NFB (no feedback). The third scenario assumes an extremely efficient dynamical feedback by invoking the condition that the latitudinal temperature gradients in the perturbed stratosphere remained unchanged at their unperturbed values for all altitudes and for all seasons. In other words, for this case, referred to in the text as EFB (efficient feedback), the stratospheric temperature change due to increased $CO_2$ is everywhere the globally averaged change computed for globally averaged (over both latitude and season) conditions. The above three scenarios, proposed by *Ramanathan and Dickinson* [1979], enable us to examine the sensitivity of tropospheric heating rates to possible changes in stratospheric temperatures.

A final important computation detail concerns the tropopause altitude, which is allowed to vary with latitude in accordance with observations. Additional details regarding the model resolution in the latitudinal and vertical directions, as well as the atmospheric parameters, are given in the appendix.

### b. *Seasonal Energy Balance Climate Model*

The seasonal energy balance climate model which we employ computes the zonal surface air temperature, for the northern hemisphere, as a function of time (or month) by solving the equation [*Lian*, 1978]

$$R(\theta)\left\{\frac{\partial T_s(\theta, t)}{\partial t} + \omega[T_s(\theta, t) - \bar{T}_s(\theta)]\right\} = S(\theta, t)[1 - \alpha(\theta, t)] - \nu[T_s(\theta, t) - \langle T_s\rangle] - F(\theta, t) - \Delta G(\theta, t) \quad (1)$$

where

$R(\theta)$ effective thermal inertia of the earth-atmosphere system (in J $m^{-2}$ $K^{-1}$);
$T_s(\theta, t)$ surface air temperature;
$\bar{T}_s(\theta)$ annually averaged zonal surface air temperature;
$\langle T_s\rangle$ hemispherically averaged surface air temperature;
$\omega$ $2\pi/\tau$, with $\tau$ equal to length of year (12 months);
$S(\theta, t)$ incoming solar radiation (in W $m^{-2}$);
$\alpha(\theta, t)$ zonal albedo;
$\nu$ dynamical transport coefficient, equal to 3.4 W $m^{-2}$ $K^{-1}$;
$F(\theta, t)$ outgoing longwave flux;
$-\Delta G(\theta, t)$ radiative heating due to increased $CO_2$.

The term on the left-hand side of (1) is the same as that employed by *Sellers* [1973], and this reflects the action of a sinusoidal surface temperature variation under the condition of a periodic steady state; i.e., the entire left-hand side of (1) approximates the time-dependent subsurface component of the surface heat flux [e.g., *Taylor*, 1976]. The dynamical transport term employed within (1) is from *Budyko* [1969]. Although this parameterization was originally intended for use within an annual climate model, we note that *Thompson and Schneider* [1979] have incorporated, within a seasonal climate model, nonlinear diffusive transport as well as Budyko transport, and they find little difference in the output of their model employing these two separate transport formulations.

For present purposes we have taken the latitudinal distribution of cloud cover to be independent of time and equal to its annual average distribution. A related study [*Lian*, 1978], per-

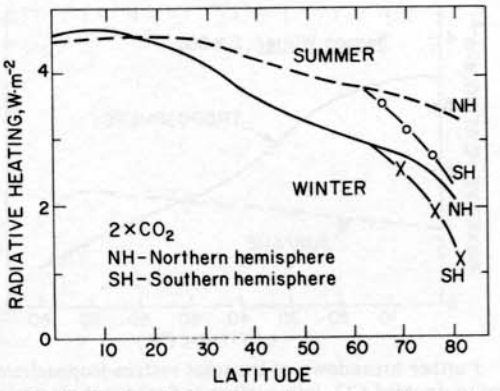


Fig. 1. Radiative heating of the surface-troposphere system due to doubled $CO_2$. Assumed present-day value of the $CO_2$ mixing ratio is 320 ppm (by volume). Change in stratospheric temperatures due to increased $CO_2$ is computed as in case NFB.

taining to climatic change induced by a change in solar constant, incorporated both annual and seasonal distributions of total cloud cover and found that these separate cloud cover prescriptions yielded nearly identical results for the time-dependent surface air temperature. The procedures for obtaining parameterizations for $\alpha(\theta, t)$ and $F(\theta, t)$, appearing within (1), as well as the evaluation of the effective thermal inertia $R$ are briefly described in the appendix; a more detailed description is given by *Lian* [1978].

The increased $CO_2$ radiative heating is given by $-\Delta G$, where $\Delta G$ is the change in the net radiative flux at the tropopause (note from previous discussion that $\Delta G$ is negative), due to increased $CO_2$, as computed from the radiative transfer model calculations. The $\Delta G$ values employed in (1) include the effects of stratospheric temperature change. Recall that we consider three scenarios for computing stratospheric temperature change, and for reasons given below we employ $\Delta G$ values computed from the NFB scenario. For use within (1), $-\Delta G$ is expressed as

$$-\Delta G = G_0(\theta) + G_1(\theta)\sin(\omega t) + G_2(\theta)\cos(\omega t) + G_3(\theta)\sin(2\omega t) + G_4(\theta)\cos(2\omega t) \quad (2)$$

where the latitudinally dependent coefficients $G_n(\theta)$ are determined by fitting to the seasonally calculated values of $-\Delta G$.

The solar heating and longwave cooling in (1), as given by the first and third terms on the right-hand side, apply for the entire vertical column, extending from the surface to the top of the atmosphere. Hence the $-\Delta G$ term in (1) should correspond to the heating of the entire vertical column. But since $\Delta G$ is the change in the net radiative flux at the tropopause, $-\Delta G$ in general would denote the heating of the surface-troposphere system and not the heating of the entire vertical column. However, as will be explained below, for the NFB case, $-\Delta G$ denotes the heating of the entire vertical column. The NFB case assumes that the perturbation in radiative heating (due to increased $CO_2$) is compensated by local radiative adjustments of stratospheric temperatures. In other words, the stratospheric temperature distribution is adjusted until the radiative heating perturbation vanishes at all altitudes within the stratosphere (cf. the discussion following (A5) in the appendix). As a result, $\Delta G$ is constant within the stratosphere, such that for the NFB case, $-\Delta G$ denotes the radiative heating of the entire vertical column, extending from the surface to the top of the atmosphere.

The procedure we adopt to compute the change in $T_s$ (due to increased $CO_2$) neglects the following two stratosphere-troposphere radiative interactions: (1) possible changes in stratospheric radiation due to changes in tropospheric and surface temperatures and (2) the coupling between tropospheric temperature increase and $CO_2$ radiative effects within the troposphere. In order to examine the magnitude of the above two processes, we recomputed the $\Delta G$ values by incorporating the change in $T_s$ computed from (1). These calculations indicated that the $-\Delta G$ values are larger by about 10% with the inclusion of the above two processes.

## 3. Radiative Heating Due to Increased $CO_2$

We consider three scenarios for increased $CO_2$; the fractional increases in $CO_2$ for these scenarios are 1.33, 1.67, and 2, where the fractional increase denotes the ratio of the $CO_2$ mixing ratio in the perturbed atmosphere to that for the unperturbed atmosphere, which is assumed to be 320 ppm. Most of the following discussions will pertain to doubled $CO_2$, and where it is appropriate, we will show results for the 1.33 and 1.67 fractional increases.

### *a. Heating of the Surface-Troposphere System*

The heating of the surface-troposphere system is given by the negative of the change in the net radiative flux at the tropopause. The summer and winter values of this heating, for doubled $CO_2$, are shown in Figure 1. The stratospheric temperature change is computed for the NFB case. The following features are revealed in Figure 1.

1. The radiative heating decreases from 4.6 W $m^{-2}$ at the equator to 2.2 W $m^{-2}$ at 80°N.

2. Northward of 20°N the heating is larger in summer than in winter, and the difference between the summer and winter heating increases with increasing latitude. At 80°N the summer heating is 3.3 W $m^{-2}$, while the winter value is 2.2 W $m^{-2}$.

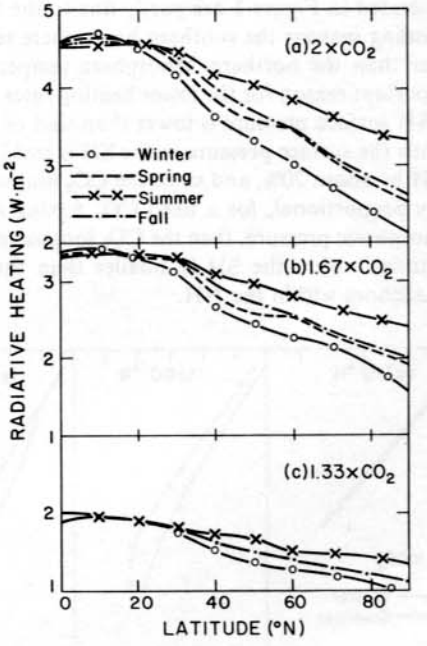


Fig. 2. Seasonal values of radiative heating of the surface-troposphere system for three cases of increased $CO_2$. The symbol $CO_2$ in the figure denotes the assumed present-day value of 320 ppm: (*a*) 2 times the present-day $CO_2$, (*b*) 1.66 times the present-day $CO_2$, and (*c*) 1.33 times the present-day $CO_2$. Stratospheric temperature change is computed as in case NFB.

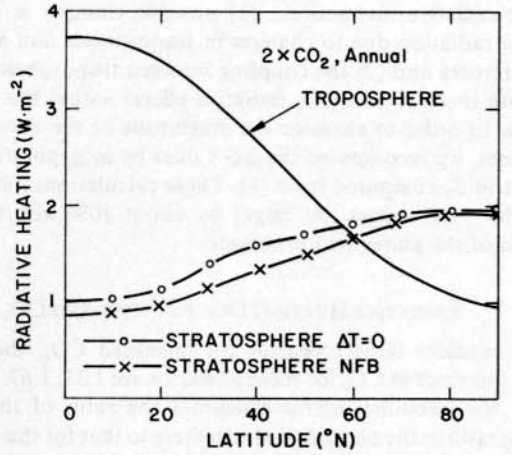


Fig. 3. Separate contributions from the troposphere and the stratosphere to the total heating of the surface-troposphere system, due to doubled $CO_2$, for annual mean conditions. The troposphere contribution is given by the reduction in the upward radiative flux at the tropopause, and the stratosphere contribution is given by the increase in the downward radiative flux from the stratosphere.

3. At high latitudes the northern hemisphere (NH) heating rates are larger than those of the southern hemisphere (SH).

The above mentioned seasonal latitudinal and interhemispheric differences in the $CO_2$ heating rates are caused by the temperature dependence of the 15-$\mu$m Planck function and that of the opacity of the $CO_2$ hot bands. Both the 15-$\mu$m Planck function and the $CO_2$ hot band opacities decrease exponentially with temperature [*Augustsson and Ramanathan*, 1977]. This temperature dependence of the $CO_2$ radiative effects, when it is considered in conjunction with the observed seasonal and latitudinal variations of the surface and tropospheric temperatures, is sufficient to explain the latitudinal and seasonal variations of the $CO_2$ heating rates shown in Figure 1. The interhemispheric differences in the high-latitude heating rates illustrated in Figure 1 are partly due to the fact that for corresponding seasons the southern hemisphere temperatures are colder than the northern hemisphere temperatures. Another important reason for the lower heating rates in the SH is that the SH surface pressure is lower than that of the NH. At 80° latitude the surface pressure in the SH is smaller than that in the NH by about 20%, and since the $CO_2$ longwave opacity is linearly proportional, for a fixed $CO_2$ mixing ratio, to the total atmospheric pressure, then the $CO_2$ longwave opacity for high latitudes within the SH is smaller than that for comparable latitudes within the NH.

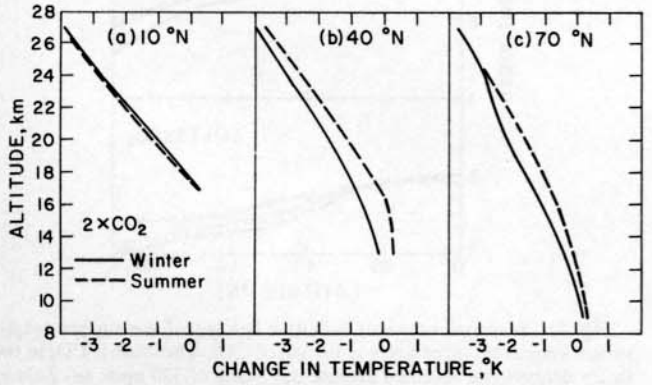


Fig. 4. Latitudinal values of the change in stratospheric temperatures (computed as in case NFB) for doubled $CO_2$: (*a*) 10°N, (*b*) 40°N, and (*c*) 70°N.

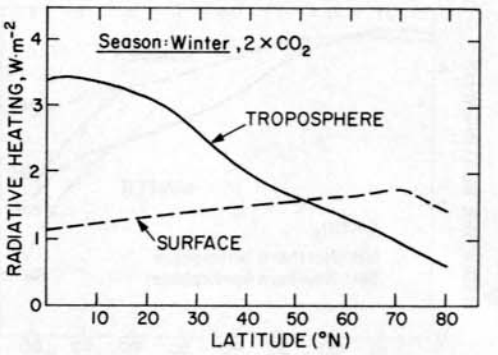


Fig. 5. Further breakdown of the total surface-troposphere heating due to doubled $CO_2$ into surface and troposphere heating.

The surface-troposphere heating for the four seasons and for the northern hemisphere is shown in Figures 2*a*, 2*b*, and 2*c* for $2 \times CO_2$, $1.67 \times CO_2$, and $1.33 \times CO_2$, respectively. The hemispheric annual mean values of $-\Delta G$ (in watts per square meter) are

$$\begin{aligned} -\langle \Delta G \rangle &= 1.72 \quad 1.33 \times CO_2 \\ -\langle \Delta G \rangle &= 3.03 \quad 1.67 \times CO_2 \\ -\langle \Delta G \rangle &= 4.12 \quad 2 \times CO_2 \end{aligned} \tag{3}$$

### b. *Stratospheric Effects on Surface-Troposphere Heating*

The surface-troposphere heating, shown in Figures 1 and 2, is in part due to the increased downward longwave emission ($\Delta F_T{}^{\downarrow}$) from the stratosphere. As has been described by *Schneider* [1975], there are two competing effects on $\Delta F_T{}^{\downarrow}$: (1) an increase in $F_T{}^{\downarrow}$ from the enhanced longwave opacity due to increased $CO_2$ and (2) a decrease in $F_T{}^{\downarrow}$ from the reduced stratospheric temperature due to increased $CO_2$ (the reasons for the decrease in stratospheric temperature are given by *Manabe and Wetherald* [1967] and *Schneider* [1975], and hence they will not be repeated here). The above stratospheric effects on the computed surface-troposphere heating are shown in Figure 3 for the $2 \times CO_2$ case.

The results of Figure 3 apply for annual mean conditions, and these show the individual contributions from the troposphere and the stratosphere to the surface-troposphere heating. The tropospheric contribution is determined from the decrease in the upward flux at the tropopause, while the stratospheric contribution corresponds to the increase in the downward flux at the tropopause. The stratospheric contribution is illustrated in Figure 3 for the following two cases: (1) the $\Delta T = 0$ curve corresponds to the case for which the stratospheric temperatures are held fixed at the unperturbed (i.e., observed) values, and (2) for the NFB curve the change in stratospheric temperatures is computed according to the NFB case. Recall that in the NFB case the stratospheric temperatures are adjusted from the unperturbed temperatures until the radiative heating (or cooling) perturbation, due to increased $CO_2$, vanishes.

From Figure 3, comparing first the tropospheric and stratospheric contributions, the stratospheric contribution increases poleward, while the converse occurs for the tropospheric contribution. The poleward increase of the stratospheric contribution is a consequence of the poleward increase of stratospheric mass (the tropopause pressure is roughly 100 mbar at the equator and 300 mbar at the north pole). The reason for the poleward decrease of the tropospheric contribution has been discussed earlier.

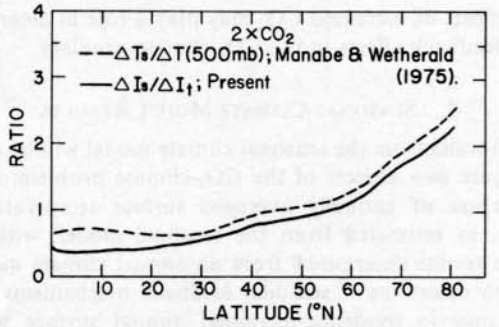


Fig. 6. Comparison of the ratio of the surface heating ($\Delta I_s$) to the troposphere heating ($\Delta I_t$) with the ratio of the increase in surface temperature ($\Delta T_s$) to the increase in 500-mbar temperature ($\Delta T$(500 mbar)), as computed by *Manabe and Wetherald*'s [1975] GCM model for doubled $CO_2$.

Comparing next the stratospheric contribution for the $\Delta T = 0$ and NFB cases, we see that the increase in the downward longwave flux is relatively insensitive to the computed change in stratospheric temperatures. This result can easily be explained from Figure 4, which shows the vertical distribution of stratospheric temperature change for three representative latitudes. As can be seen from Figure 4, the temperature change is relatively small ($\lesssim 1°K$) within the first 5 km above the tropopause. Furthermore, most ($\approx 70\%$) of the contribution to the increased downward longwave flux at the tropopause comes from the region within 5 km above the tropopause. Since the temperature change in this region is small, the increased downward flux at the tropopause is relatively insensitive to the computed changes in stratospheric temperatures. We also computed the stratospheric contribution to the surface-troposphere heating for the EFB case, in which we impose globally averaged stratospheric temperature change at all latitudes; the results for this case are almost identical to those shown in Figure 3 for the NFB case. Since, as was mentioned in the introduction, the NFB and EFB cases provide two extreme scenarios for the possible influence of dynamical feedback processes on the computed changes in stratospheric temperature, we conclude that our results for the surface-troposphere heating are insensitive to dynamical processes.

### c. *Differences Between Surface and Tropospheric Heating Rates*

The radiative heating due to doubled $CO_2$ is shown separately for the surface and the troposphere in Figure 5. We show only winter values, since the relative difference between the surface and tropospheric heating rates for the other seasons is similar to that shown in Figure 5. Note that for low latitudes the tropospheric heating is larger than the surface

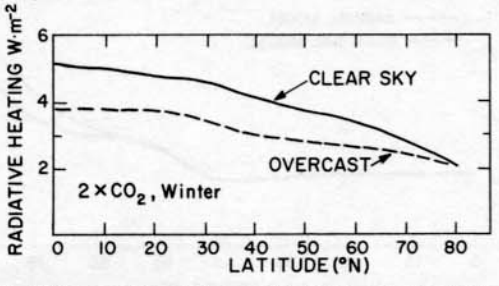


Fig. 7. Winter values of the doubled $CO_2$ heating of the surface-troposphere system for clear sky and overcast sky conditions. The overcast sky values denote an average over low, middle, and high clouds.

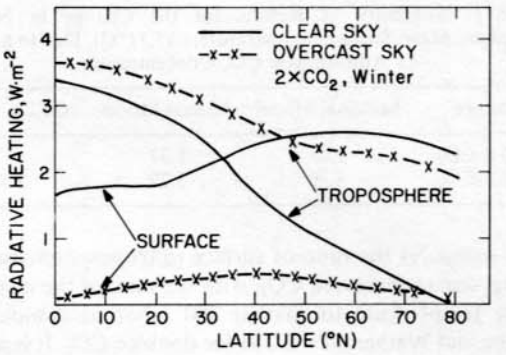


Fig. 8. Same as Figure 7, but the surface-troposphere heating is broken down into surface heating and tropospheric heating.

heating, while the converse occurs at high latitudes. The reason for this is as follows. The $CO_2$ bands within the 12- to 18-$\mu$m region are overlapped by $H_2O$ bands, and hence enhanced emission by tropospheric $CO_2$ is partly absorbed within the troposphere by $H_2O$. This $H_2O$ absorption of increased $CO_2$ emission enhances the tropospheric heating, which is accompanied by a corresponding decrease in surface heating due to part of the increased downward emission by tropospheric $CO_2$ being absorbed within the troposphere by $H_2O$. This $H_2O$ influence on the $CO_2$ heating is a maximum at the equator and a minimum at the poles because of the latitudinal variation of $H_2O$ amount within the troposphere.

On the basis of the results shown in Figure 5 it is possible to speculate on feedback mechanisms by which an increase in $CO_2$ can warm the surface. At low latitudes the direct radiation effect of increased $CO_2$ is to increase primarily the tropospheric temperature, whereas, as will be explained below, the surface warming is produced by atmospheric feedback processes. Since the troposphere tends to conserve relative humidity, the tropospheric $H_2O$ content would increase with increased tropospheric temperature, with both effects, resulting from increased $CO_2$, enhancing the tropospheric downward longwave emission to the surface. From the results shown by *Manabe and Wetherald* [1975], we estimate that this enhancement in downward longwave emission (resulting from the increased tropospheric temperature and humidity) is significantly more important for warming the surface than the increased $CO_2$ surface heating. For example, with a doubling of $CO_2$, Manabe and Wetherald's general circulation model (GCM) estimates an increase in surface temperature of 2.0°–2.5°K within equatorial regions. From Figure 5 the surface heating of 1.1 W m$^{-2}$ at the equator, due to the direct radiative effects of doubled $CO_2$, can cause a maximum surface warming of about 0.2°K, and hence roughly 90% of the 2.0°–2.5°K surface warming obtained by the GCM is caused by the atmospheric feedback processes described above. (The 0.2°K surface warming is obtained by making the extreme assumption that the surface heating is balanced solely by radiative emission of the surface. In reality, however, a part of the heating will be compensated by cooling due to enhanced evaporation from the warmer surface.) On the other hand, at high latitudes, as shown in Figure 5, the primary effect of increased $CO_2$ is to warm the surface (rather than the troposphere), and this surface warming may be amplified by ice albedo and lapse rate feedback processes [*Manabe and Wetherald*, 1975; *Ramanathan*, 1977].

An additional point raised by the results of Figure 5 concerns the direct radiative effect of increased $CO_2$ on the lapse rate of the troposphere. This point is illustrated in Figure 6,

TABLE 1. Summary of Results for the Change in Northern Hemisphere Mean Surface Temperature, $\langle \Delta T_s \rangle$ (°C), Due to a Change in Atmospheric $CO_2$ Concentration

| Change | Seasonal Model | Annual Model | GFDL GCM |
|---|---|---|---|
| $1.33 \times CO_2$ | 1.45 | 1.37 | ... |
| $2 \times CO_2$ | 3.32 | 3.29 | 2.93 |

which compares the ratio of surface to tropospheric radiative heating, due to increased $CO_2$, with the ratio of the increase in surface temperature to that at 500 mbar as computed by Manabe and Wetherald's GCM for doubled $CO_2$. It is particularly striking that the latitudinal variations of the two ratios are similar. As is evident from Figure 6, the lapse rate in Manabe and Wetherald's model decreased in the tropics and increased at high latitudes. Manabe and Wetherald explain that the decrease in lapse rate at low latitudes is due to moist convective processes which tend to stabilize the troposphere for an increase in surface temperature. Manabe and Wetherald further indicate that the large increase in polar temperatures (due to ice albedo feedback) is restricted to the region close to the surface (due to the fact that vertical mixing processes are weak at high latitudes). Consequently, the lapse rate at high latitudes increases with an increase in surface temperature. However, the results of Figure 6 suggest that the latitudinal distributions of surface and tropospheric $CO_2$ heating rates may partly be responsible for the latitudinal distribution of the computed lapse rate changes.

### d. *Clear and Overcast Heating Rates*

Figure 7 shows the clear sky and overcast sky heating due to increased $CO_2$ for the surface-troposphere system, while Figure 8 shows these quantities for the surface and troposphere separately. These results again correspond to winter conditions. The overcast sky heating rates were obtained by taking the difference of the total heating rate from the clear sky heating rate and dividing this difference by the total cloud cover. Hence the overcast sky heating rates shown in Figure 7 should represent an average effect for the three-level clouds employed in this study.

From Figure 7 the overall heating of the surface-troposphere system is smaller for the overcast case, and the difference between the clear and overcast cases is greatest at the equator, where the heating rate for the overcast case is smaller by about 30%. Figure 8 reveals the following interesting features.

1. The tropospheric heating rates are larger for overcast conditions, whereas the surface heating is larger for clear sky conditions.
2. The difference between overcast and clear sky heating rates increases poleward, and at 80° the clear sky tropospheric heating nearly vanishes.
3. The heating of the surface due to increased $CO_2$ is negligible for overcast conditions.

The above differences between clear and overcast heating rates attain their maximum values at high latitudes. For 80° the tropospheric heating is 2 W $m^{-2}$ for overcast conditions and 0 for clear sky conditions, whereas the surface heating is almost 0 for overcast conditions and 2.2 W $m^{-2}$ for clear sky conditions. It follows that increased $CO_2$ causes a change in the differences between the clear and overcast radiation energy balances, and this change is as large as the total effect of increased $CO_2$ on the surface-troposphere energy balance. Such effects of increased $CO_2$ may play a role in determining cloud feedback effects in the $CO_2$-climate problem.

## 4. Seasonal Climate Model Results

The results from the seasonal climate model will be used to investigate two aspects of the $CO_2$-climate problem: (1) the comparison of annually averaged surface temperature increases, as estimated from the seasonal model, with comparable results determined from an annual climate model in order to determine if seasonal feedback mechanisms are of importance in modeling-increased annual surface temperatures due to enhanced $CO_2$ and (2) to specifically illustrate seasonal enhancements in surface temperature resulting from increased $CO_2$.

### a. *Annual Average Surface Temperatures*

In that ice albedo feedback comprises a nonlinear interactive feedback mechanism, we might anticipate that the seasonal variability in $CO_2$ radiative heating, as has been previously discussed and illustrated in Figures 1 and 2, might interact with ice albedo feedback to produce annually averaged surface temperatures which differ significantly from those predicted by an annual climate model. To appraise such a possibility, we have evaluated the increase in seasonal zonal surface temperature $\Delta T_s(\theta, t)$, due to increased $CO_2$, with subsequent annual averaging to determine the zonal annual increase $\Delta \bar{T}_s(\theta)$ and the hemispheric annual increase $\langle \Delta T_s \rangle$ for the northern hemisphere. We next evaluated both $\Delta \bar{T}_s(\theta)$ and $\langle \Delta T_s \rangle$ by using our climate model as an annual model. The present seasonal model, when it is employed as an annual model, is essentially the same as that described by *Lian and Cess* [1977] and with (2) replaced by the annually averaged quantity $-\Delta \bar{G}(\theta)$.

Consider first $\langle \Delta T_s \rangle$ as determined from both the seasonal model and the annual model. Results for the increase in hemispheric mean temperature are summarized in Table 1 for $1.33 \times CO_2$ and $2 \times CO_2$. Surprisingly, there is little difference between the seasonal model and the annual model estimates, suggesting that the seasonal variability of the $CO_2$ radiative heating, $-\Delta G$ in (1), does not play a significant interactive role as far as hemispheric mean surface temperature is concerned. Also shown in Table 1 is the $2 \times CO_2$ result of *Manabe and Wetherald* [1975], obtained from the Geophysical Fluid Dynamics Laboratory GCM (GFDL GCM), which is also an annual model. The agreement of our results with those of the GFDL GCM is quite satisfactory.

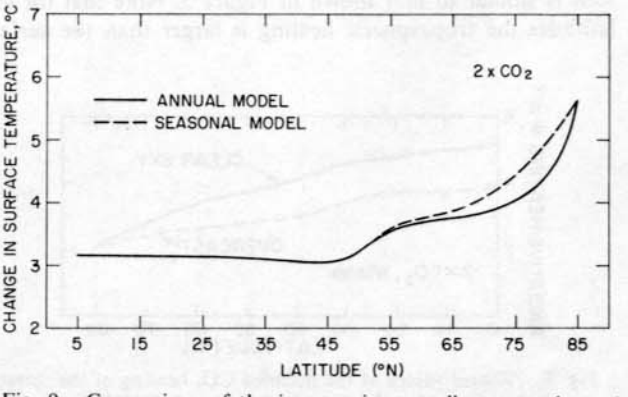


Fig. 9. Comparison of the increase in annually averaged zonal surface temperature, due to doubled $CO_2$, as computed by seasonal and annual energy balance climate models.

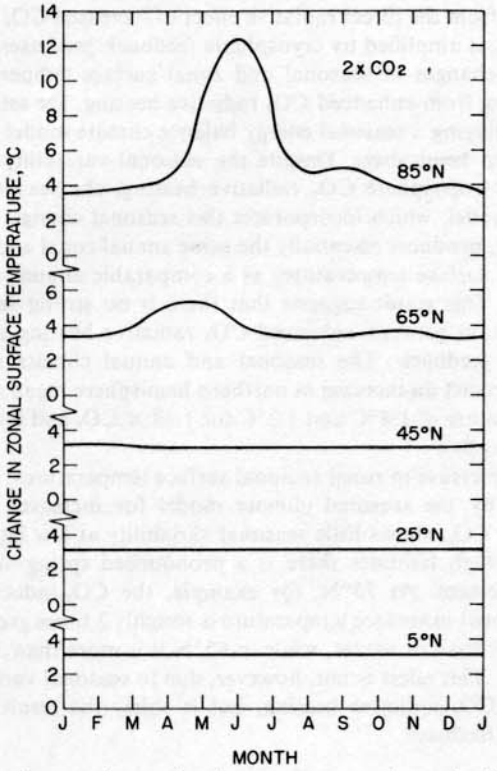


Fig. 10. Increase in zonal surface temperature, due to doubled $CO_2$, as a function of month for several latitudes.

Our conclusion that the seasonal variability of $-\Delta G$ has no significant effect upon $\langle \Delta T_s \rangle$ can also be extended to the latitudinal variability of $-\Delta G$; the latitudinal variability of the $CO_2$ radiative heating is also shown in Figures 1 and 2. To illustrate this, from a hemispheric energy balance

$$\langle \Delta T_s \rangle = -\frac{\langle \Delta G \rangle}{\langle dF/dT_s \rangle} \Gamma \tag{4}$$

where $\Gamma$ is the enhancement factor due to ice albedo feedback, which we choose to be the same as that for a solar constant change; $\Gamma = 1.25$ from *Lian and Cess* [1977]. Evaluating $\langle dF/dT_s \rangle$ from (A6), while $\langle \Delta G \rangle$ values are given by (3), then

$$\begin{aligned} \langle \Delta T_s \rangle &= 1.34°\text{C} \qquad 1.33 \times CO_2 \\ \langle \Delta T_s \rangle &= 3.22°\text{C} \qquad 2 \times CO_2 \end{aligned} \tag{5}$$

These hemispheric estimates of $\langle \Delta T_s \rangle$ are in essentially precise agreement with the annual zonal model estimates of Table 1, indicating that the latitudinal variability of the annually averaged $CO_2$ radiative heating, $-\Delta G(\theta)$, plays no significant role with regard to the increase in hemispheric temperature due to increased $CO_2$.

In that similar estimates for $\langle \Delta T_s \rangle$ are obtained from either an annual or seasonal zonal climate model (Table 1), we might expect that results for the increase in annual zonal surface temperature, $\Delta \hat{T}_s(\theta)$, from the two models would also be similar. Figure 9 shows a comparison of $\Delta T_s(\theta)$, as determined from both models with $2 \times CO_2$, which indicates that our expectation is correct. At least within the confines of our present modeling there is no evidence that seasonal variability in the $CO_2$ radiative heating plays a significant interactive role with respect to model estimates of the $CO_2$-induced increase in annual surface temperatures.

### b. *Seasonal Surface Temperatures*

Although the present climate model comparisons do not indicate any significant seasonal interactions with regard to the increase in either $\langle \Delta T_s \rangle$ or $\Delta \hat{T}_s(\theta)$, due to increased $CO_2$, there are some interesting seasonal effects. In Figure 10 we illustrate the seasonal increase of zonal surface temperature, $\Delta T_s(\theta, t)$, for several latitude zones and for doubled $CO_2$. At the lower latitudes there is essentially no seasonal variability in the zonal temperature increase, but at high latitudes there is a pronounced enhancement in $\Delta T_s(\theta, t)$ which occurs during the spring at 65°N and during the spring/summer at 85°N. In Figure 11 we present results for a greater number of high-latitude zones, as well as for both $1.33 \times CO_2$ and $2 \times CO_2$. This figure illustrates that the magnitude of the spring/summer enhancement in $\Delta T_s(\theta, t)$ increases monotonically with increasing latitude. At 75°N the $CO_2$-induced enhancement in surface temperature is roughly 2 times as great in summer as compared with winter, while at 85°N this factor is greater than 3. The high-latitude summer enhancement in surface temperature could be of considerable importance with regard to the stability of arctic sea ice.

At first sight, it would appear that the spring/summer surface temperature enhancement is due to $-\Delta G$ being a maximum during the summer (see Figures 1 and 2). But to test this, we ran the seasonal model with annually averaged zonal values for $-\Delta G$ and obtained essentially the same results (within 0.1°C) as those of Figure 11. The sole reason for the high-latitude spring/summer surface temperature enhancement is seasonal ice albedo feedback.

For the present model, ice albedo feedback acts only when $T_s(\theta, t) < 0$°C (see the appendix), where $T_s(\theta, t)$ is the zonal seasonal temperature. But ice albedo feedback also requires the presence of solar radiation, which is either small or absent at high latitudes during the winter. Thus the winter change in

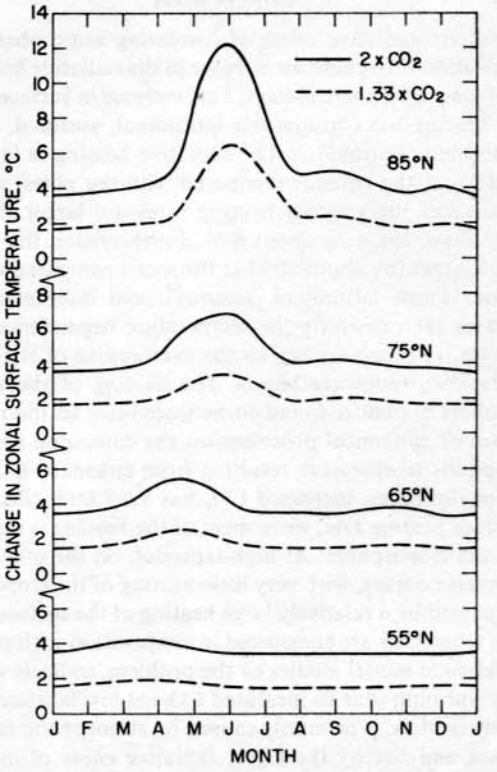


Fig. 11. Same as Figure 10 but for a larger number of high latitudes and for both $1.33 \times CO_2$ and $2 \times CO_2$.

high-latitude zonal surface temperature, $\Delta T_s(\theta, t)$, due to increased $CO_2$, is about the same as that at low latitudes, where ice albedo feedback is also absent, since $T_s(\theta, t) > 0°C$. The spring/summer enhancement in high-latitude $\Delta T_s(\theta, t)$ is consequently due to increasing ice albedo feedback with increasing seasonal insolation; the maximum enhancement corresponds roughly to $T_s(\theta, t) = 0°C$ for the enhanced $CO_2$ cases. The reduction in $\Delta T_s(\theta, t)$, following the maximum, is thus the result of ice albedo feedback continuing to amplify the present $CO_2$ seasonal surface temperatures, but not those for enhanced $CO_2$.

Quite obviously, there are numerous time-dependent processes which have been ignored within the model, and the present results should only be interpreted as being suggestive of substantial high-latitude spring/summer increases in surface temperature due to increased atmospheric $CO_2$. But the results of Figures 10 and 11 are quite consistent with snow and ice melting progressively later in the year as latitude increases.

Significantly different results, however, have been obtained by *Sellers* [1974]. He finds the largest model increase in $\Delta T_s(\theta, t)$, for increased $CO_2$, to occur at 75°–85°N for December/January. Since this corresponds to the polar night, Sellers' high-latitude surface temperature amplification cannot be directly due to ice albedo feedback. Evidently, there is some other high-latitude feedback mechanism within his model.

A final point regarding the results of Figure 11 concerns the ability to actually detect, at some future time, climatic warming due to increased atmospheric $CO_2$. The difficulty here lies in the capability to actually detect a '$CO_2$ signal' above natural climatic noise. The present seasonal results suggest that such a signal should first appear during high-latitude summers. For example, with $1.33 \times CO_2$ our present estimate for the increase in northern hemisphere mean surface temperature is 1.45°C, whereas for June at 85°N it is 6.5°C.

## 5. Conclusions

The direct radiative effect of increasing atmospheric $CO_2$ concentration is to cause an increase in the radiative heating of the surface-troposphere system. This increase in surface-troposphere heating has considerable latitudinal, seasonal, and interhemispheric variability. The radiative heating is larger by about 60% at the equator compared with the poles, while at high latitudes the summer heating rates are larger than the winter values, again by about 60%. Furthermore, the heating rates are larger (by about 50%) at the arctic compared with the antarctic. These latitudinal, seasonal, and interhemispheric differences are caused by the temperature dependence of the $CO_2$ radiative processes and by the overlapping of $H_2O$ bands with the $CO_2$ longwave bands. The heating of the surface-troposphere system is found to be insensitive to the possible influence of dynamical processes on the computed change in stratospheric temperature resulting from enhanced $CO_2$.

At low latitudes, increased $CO_2$ has very little effect upon the surface heating rate, since most of the heating is deposited within the troposphere. At high latitudes, on the other hand, the converse occurs, with very little heating of the troposphere accompanied by a relatively large heating of the surface. These results, when they are considered in conjunction with previous GCM-climate model studies of the problem, indicate that the surface warming (due to increased $CO_2$) at low latitudes, computed by models, is primarily caused by atmospheric feedback processes and not by the direct radiative effect of increased $CO_2$. On the other hand, the surface warming at high latitudes results from the direct radiative effect of increased $CO_2$ which, in turn, is amplified by cryospheric feedback processes.

The changes in seasonal and zonal surface temperatures, resulting from enhanced $CO_2$ radiative heating, are estimated by employing a seasonal energy balance climate model for the northern hemisphere. Despite the seasonal variability of the surface-troposphere $CO_2$ radiative heating, the seasonal climate model, which incorporates this seasonal change in $CO_2$ heating, produces essentially the same annual zonal and hemispheric surface temperatures as a comparable annual climate model. This result suggests that there is no strong seasonal interaction between enhanced $CO_2$ radiative heating and ice albedo feedback. The seasonal and annual climate models both predict an increase in northern hemisphere mean surface temperature of 1.4°C and 3.2°C for $1.33 \times CO_2$ and $2 \times CO_2$, respectively.

The increase in zonal seasonal surface temperatures, as predicted by the seasonal climate model for increased atmospheric $CO_2$, shows little seasonal variability at low latitudes, but at high latitudes there is a pronounced spring/summer enhancement. At 75°N, for example, the $CO_2$-induced enhancement in surface temperature is roughly 2 times greater in summer than in winter, while at 85°N it is more than 3 times greater. This effect is not, however, due to seasonal variability of the $CO_2$ radiative heating, but is solely the result of ice albedo feedback.

## Appendix

### a. *Radiative Transfer Model*

The radiative transfer model used in this study is described by ***Ramanathan and Dickinson*** [1979], and this constitutes an improved version of the model developed by ***Ramanathan*** [1976]. The following is a list of some of the major improvements.

1. The longwave cooling rates are calculated by computing the upward and downward fluxes at the interface of each model layer and then taking the flux difference across the layer.
2. The present model has three cloud layers instead of one.
3. The additional $CO_2$ hot bands in the 12- to 18-$\mu$m region, described by ***Augustsson and Ramanathan*** [1977], are included.
4. A more accurate procedure is adopted for diurnal averaging of solar heating.
5. The stratospheric temperature is calculated by a time-marching technique in which we solve an equation of the form

$$\partial T/\partial t = Q \tag{A1}$$

where $Q$ is the net heating rate. In the present analysis we are concerned only with the change of stratospheric temperature from the observed value, due to $CO_2$ increase; hence (A1) is written as

$$\partial T'/\partial t = \Delta Q' \tag{A2}$$

where

$$T' = T - T^\circ \tag{A3}$$

$$\Delta Q' = Q(T) - Q(T^\circ) \tag{A4}$$

with $T^\circ$ denoting the observed temperature, while $Q(T)$ is the net heating rate of the perturbed stratosphere and $Q(T^\circ)$ that of the observed stratosphere. The differential equation (A2) is solved by letting

TABLE 2. Observed Distributions of Atmospheric Parameters Adopted for the Calculations

| Parameter | Reference |
|---|---|
| Temperature | 0–20 km from *Oort and Rasmusson* [1971]<br>20–54 km. from Cira (1972) |
| Humidity | *Oort and Rasmusson* [1971] |
| Clouds | *London* [1957] |
| Ozone | *Dütsch* [1969] |

$$T_c' = T_p' + \Delta Q' \, \Delta t \tag{A5}$$

where $T_c'$ and $T_p'$ are the temperatures at the current and previous time steps, respectively, with $\Delta t = 6$ hours. Equation (A5) is marched in time until $\Delta Q'$ is zero at all levels within the stratosphere. For computational purposes the condition $\Delta Q' = 0$ is replaced by $|\Delta Q'| \leq 5 \times 10^{-5}$ °K/d.

The model extends in the vertical direction from the ground to 54 km in altitude and has 24 layers. Below 30 km, each layer is 2 km thick, while above 30 km the layers are 3 km thick. In the latitudinal direction there are nine equally spaced latitude points at 10° intervals between 0° and 80°. Atmospheric pressure, temperature, clouds, humidity, and ozone are specified as a function of season, latitude, and altitude, based upon observed zonally averaged climatological values for the northern hemisphere; the references for the observed data are given in Table 2. The surface and cloud albedos are allowed to vary with zenith angle as prescribed by *Lian and Cess* [1977] and *Cess* [1976], respectively, while emissivities of clouds are those suggested by *Cess and Ramanathan* [1978].

*b. Seasonal Climate Model*

The seasonal energy balance climate model used in this study is described in detail by *Lian* [1978], so that here we give only a brief description of the model, together with the parameterizations of $F(\theta, t)$ and $\alpha(\theta, t)$ for use in (1). As was discussed in the text, we take the zonal cloud cover fractions to be the annual mean values, since in a related study [*Lian*, 1978] the output of the seasonal model, for a change in solar constant, was independent upon use of either annual or seasonal cloud cover fractions. In the following, we let $A_c(\theta)$ denote the annual mean cloud cover fraction for a given latitude zone, with these values taken from *London* [1957]. The parameterization of $F(\theta, t)$, for use within (1), is taken from *Cess* [1976], such that $F$ is expressed in terms of $T_s(\theta, t)$ and $A_c(\theta)$ as

$$F(W\,m^{-2}) = 257 - 91A_c(\theta) + 1.6T_s(\theta, t) \tag{A6}$$

with $T_s$ in degrees Celsius.

To formulate a seasonal parameterization for the zonal albedo $\alpha_s(\theta, t)$, we first consider the clear sky albedo $\alpha_s(\theta, t)$ and represent this as

$$\alpha_s(\theta, t) = b(\theta) + \left(\frac{\partial \alpha_s}{\partial \mu}\right)\mu(\theta, t) + \left(\frac{\partial \alpha_s}{\partial T_s}\right)T_s(\theta, t) \tag{A7}$$

The quantity $b(\theta)$ is described later. The second term in the above expression denotes the seasonal variation of clear sky albedo due to seasonal changes in solar zenith angle, with $\mu =$ cos (zenith angle), and $\partial \alpha_s / \partial \mu$ is taken as the annual mean value and evaluated as by *Lian and Cess* [1977]. The final term in (A7) represents ice albedo feedback, with $\partial \alpha_s / \partial T_s$ taken to be zero for $T_s > 0$°C, whereas for $T_s \leq 0$°C it is assumed to be independent of time. Although annual mean values of $\partial \alpha_s / \partial T_s$ have been determined by *Lian and Cess* [1977] as a function of latitude, we would not expect these annual quantities to be representative of the seasonal $\partial \alpha_s / \partial T_s$ values.

There does, however, appear to be a simple means of relating these two separate quantities. Letting $\bar{\alpha}_s(\theta)$ and $\bar{S}(\theta)$ represent the zonal annual clear sky albedo and insolation, respectively, then

$$\bar{\alpha}_s(\theta) = \frac{1}{\tau \bar{S}(\theta)} \int_0^\tau S(\theta, t)\alpha_s(\theta, t)\, dt \tag{A8}$$

In that $\bar{\alpha}_s(\theta)$ will depend upon $\bar{T}_s(\theta)$, where $\bar{T}_s(\theta)$ is the annually averaged zonal surface temperature, while $\alpha_s(\theta, t)$ is dependent upon the seasonal surface temperature $T_s(\theta, t)$, it follows that

$$\frac{\partial \bar{\alpha}_s}{\partial \bar{T}_s} = \frac{1}{\tau \bar{S}(\theta)} \int_0^\tau S(\theta, t) \frac{\partial \alpha_s}{\partial T_s} \frac{dT_s}{d\bar{T}_s} d\tau \tag{A9}$$

with $dT_s(\theta, t)/d\bar{T}_s(\theta)$ denoting the change in zonal seasonal temperature as induced by a change in zonal average temperature. Due to seasonal feedback processes which are dependent upon $\bar{T}_s(\theta)$, the quantity $dT_s/d\bar{T}_s$ is not equal to unity.

Recalling that $\partial \alpha_s / \partial T_s$ is taken to be zero for $T_s(\theta, t) > 0$°C, whereas for $T_s \leq 0$°C it is assumed to be independent of time, then (A9) may be recast as

$$\frac{\partial \alpha_s}{\partial T_s} = B \frac{\partial \bar{\alpha}_s}{\partial \bar{T}_s} \tag{A10}$$

where

$$B = \left\{\frac{1}{\tau \bar{S}(\theta)} \int_{t_1}^{t_2} S(\theta, t) \frac{dT_s}{d\bar{T}_s} dt\right\}^{-1} \tag{A11}$$

with $t_1$ and $t_2$ denoting the times within the fall and the spring, respectively, when $T_s = 0$°C, since the integration within (All) is performed only for $T_s(\theta, t) \leq 0$°C. The method of evaluating $t_1$ and $t_2$, as well as $dT_s/d\bar{T}_s$, will be described shortly. The expression given by (A10) thus provides a means of converting the $\partial \bar{\alpha}_s / \partial \bar{T}_s$ results of *Lian and Cess* [1977] to $\partial \alpha / \partial T_s$ for use within the present seasonal model.

Combination of (A7), (A9), and (A10) yields the requisite result for $\alpha_s(\theta, t)$. To convert this clear sky albedo to the actual zonal albedo, we employ the standard formulation

$$\alpha(\theta, t) = \alpha_s(\theta, t)[1 - A_c(\theta)] + \alpha_c(\theta, t)A_c(\theta) \tag{A12}$$

where $\alpha_c$ is the cloudy sky albedo. This in turn is related to the clear sky albedo and zenith angle by employing [*Lian and Cess*, 1977]

$$\alpha_c = 0.64 + 0.26\alpha_s - 0.49\mu \tag{A13}$$

Combination of (A7), (A12), and (A13) thus yields $\alpha(\theta, t)$ as required for use within (1).

It is important to note that the present ice albedo feedback parameterization is applicable solely for the purpose of evaluating a change in climatic state, as opposed to predicting the present seasonal climate, since $dT_s/d\bar{T}_s$ appearing within (A10) refers to a change in zonal seasonal temperature as induced by a change in zonal annual temperature. Since $t_1$, $t_2$, and $dT_s/d\bar{T}_s$ are not known a priori, these quantities are determined through an iterative solution of (1). The model is simultaneously tuned to the present seasonal climate by letting $b(\theta)$ (A7) and $R(\theta)$ in (1) be zonally adjustable parameters. These are then evaluated from the model by minimizing the rms error in the model-predicted $T_s(\theta, t)$ results, as compared

with the observed monthly surface air temperatures of *Crutcher and Meserve* [1970]. As is discussed by *Lian* [1978], the model-produced $b(\theta)$ and $R(\theta)$ results are quite consistent with estimates by other means.

*Acknowledgments.* This work was supported in part by National Science Foundation grant ENG-7682547 to the State University of New York at Stony Brook. The National Center for Atmospheric Research is sponsored by the National Science Foundation.

## REFERENCES

Augustsson, T., and V. Ramanathan, A radiative-convective model study of the $CO_2$ climate problem, *J. Atmos. Sci., 34*, 448–451, 1977.

Budyko, M. I., The effect of solar radiation variations on the climate of the earth, *Tellus, 21*, 611–619, 1969.

Cess, R. D., Climate change: An appraisal of atmospheric feedback mechanisms employing zonal climatology, *J. Atmos. Sci., 33*, 1831–1843, 1976.

Cess, R. D., and V. Ramanathan, Averaging of infrared cloud opacities for climate modeling, *J. Atmos. Sci., 35*, 919–922, 1978.

Crutcher, H. L., and J. M. Meserve, Selected-level heights, temperatures and dew point temperatures for the northern hemisphere, *Navair 50-IC-52*, NOAA, Environ. Data Serv., Washington, D. C., 1970.

Dütsch, J. U., Atmospheric ozone and ultraviolet radiation, in *World Survey of Climatology*, vol. 4, edited by D. F. Rex, pp. 383–430, Elsevier, New York, 1969.

Lee, S. P., and F. M. Snell, An annual zonally averaged global climate model with diffuse cloudiness feedback, *J. Atmos. Sci., 34*, 847–853, 1977.

Lian, M. S., Energy balance climate models and climate sensitivity, Ph.D. thesis, State Univ. of N. Y., Stony Brook, 1978.

Lian, M. S., and R. D. Cess, Energy-balance climate models: A reappraisal of ice-albedo feedback, *J. Atmos. Sci., 34*, 1058–1062, 1977.

London, T., A study of the atmospheric heat balance, final report, contract AF19(122)-165, N. Y. Univ., New York, 1957.

Manabe, S., and R. T. Wetherald, Thermal equilibrium of the atmosphere with a given distribution of relative humidity, *J. Atmos. Sci., 24*, 241–259, 1967.

Manabe, S., and R. T. Wetherald, The effects of doubling the $CO_2$ concentration on the climate of a general circulation model, *J. Atmos. Sci., 32*, 3–15, 1975.

Ohring, G., and S. Adler, Some experiments with a zonally averaged climate model, *J. Atmos. Sci., 35*, 186–205, 1978.

Oort, A. H., and G. M. Rasmusson, *Atmospheric Circulation Statistics, NOAA Prof. Pap. 5*, U.S. Government Printing Office, Washington, D. C., 1971.

Ramanathan, V., Radiative transfer within the earth's troposphere and stratosphere: A simplified radiative-convective model, *J. Atmos. Sci., 33*, 1330–1346, 1976.

Ramanathan, V., Interactions between ice-albedo lapse-rate and cloud-top feedbacks: An analysis of the nonlinear response of a GCM climate model, *J. Atmos. Sci., 34*, 1885–1897, 1977.

Ramanathan, V., and R. E. Dickinson, The role of stratospheric ozone in the zonal and seasonal radiative energy balance of the earth-troposphere system, *J. Atmos. Sci.*, in press, 1979.

Schneider, S. H., On the carbon dioxide–climate confusion, *J. Atmos. Sci., 32*, 2060–2066, 1975.

Sellers, W. D., A new global climate model, *J. Appl. Meteorol., 12*, 241–254, 1973.

Sellers, W. D., A reassessment of the effect of $CO_2$ variations on a simple global climate model, *J. Appl. Meteorol., 13*, 831–833, 1974.

Taylor, K., The influence of subsurface energy storage on seasonal temperature variations, *J. Appl. Meteorol., 15*, 1129–1138, 1976.

Thompson, S. L., and S. H. Schneider, Seasonal simulation with a zonal energy balance climate model: A verification test of the performance of mean annual models, *J. Geophys. Res.*, in press, 1979.

(Received October 5, 1978;
revised January 11, 1978;
accepted January 29, 1978.)